ARTICLE IN PRESS

Ceramics International xxx (xxxx) xxx–xxx

Contents lists available at ScienceDirect

Ceramics International

journal homepage: www.elsevier.com/locate/ceramint

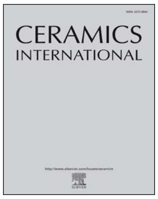

Optical and ferromagnetic properties of hydrothermally synthesized CeO_2/CuO nanocomposites

Xiaojun Ma, Ping Lu, Ping Wu*

Department of Applied Physics, Institute of Advanced Materials Physics, Tianjin Key Laboratory of Low Dimensional Materials Physics and Preparing Technology, Faculty of Science, Tianjin University, Tianjin 300354, People's Republic of China

ARTICLE INFO

Keywords:
B. Nanocomposites
C. Magnetic properties
C. Optical properties
CeO_2/CuO

ABSTRACT

Nanostructured CeO_2/CuO composites are synthesized using a facile hydrothermal reaction. Results signify that Cu ions prefer to enter into CeO_2 lattice forming solid solution at low concentration, and would be transformed into CuO phase at moderate concentration. Moreover, the addition of CuO species into CeO_2 promotes the reduction of Ce^{4+} and the creation of oxygen vacancy (V_O) defects. Raman analyses confirm V_O concentration initially increases and then decreases with the increasing CuO phase and the sample Ce1Cu2 exhibits the highest defect concentration. The room temperature ferromagnetic behavior is observed firstly in CeO_2/CuO non-magnetic system and the maximal saturation magnetization appears in Ce1Cu2. The emergent ferromagnetism appears to be relevant to the extensive V_O defects, which can be interpreted by the indirect double-exchange model. The synthetic interaction between CeO_2 and CuO results in the redshift of the bandgap in prepared CeO_2/CuO nanocomposites.

1. Introduction

Heterostructures composed of binary metal oxides not only utilize the exceptional properties of two components, but also show unexpected properties due to synergetic effects between their individual constituents [1–4]. For instance, Saravanan et al. demonstrated that synthesized CeO_2/CuO composites exhibit higher efficient visible light photocatalytic activities than pure CeO_2 or CuO [5]. Hence, CeO_2 combined with CuO has recently attracted tremendous attention and been suggested for technological applications like photocatalysts, electrocatalysts and energy transfer devices [5–8]. When two different compounds are coupled, novel properties will occur resulting from strong interactions of two phases at the interfaces [9,10]. Hence, interface engineering and structural modification are absolutely necessary to tune the physical properties in heterogeneous nanocomposites. Although several techniques, such as thermal decomposition [5], hydrothermal [6], sol-gel [7], combustion [8] and co-precipitation [11], have been developed to construct CeO_2/CuO composite nanostructures, there remains challenges on the controllable synthesis of well-defined interfaces in CeO_2/CuO nanocomposites by a hydrothermal process without any template or surfactant. Importantly, the hydrothermal approach can be easily scaled up and applied to the synthesis of other nanocomposite systems in a mild condition [6,12].

Recently, the abnormal room temperature ferromagnetism (RTFM) has been observed at interfaces in heterogeneous composites composed of two antiferromagnetic oxides or even an antiferromagnetic and a paramagnetic oxide [9,13,14]. Many groups have obtained the unexpected RTFM in nonmagnetic composites such as CuO/Cu_2O [13,14], ZnO/Al_2O_3 [15], ZnO/Co_3O_4 [16], CuO/ZnO [9,17,18], and MnO_2/ZnO [19]. For heterogeneous CeO_2/CuO nanocomposite, its optical, electronic and catalytic properties have been studied in a large amount. However, to the best of our knowledge, there is no research available on its ferromagnetic property. Investigating the ferromagnetic behavior in CeO_2/CuO nanocomposite is beneficial for various applications in spintronic and magneto-optic devices. In addition, it is still not clear about the origin of RTFM in such nonmagnetic nanocomposite systems. For example, Lu et al. have reported the point defects at interfaces play a significant role in triggering ferromagnetism in CuO/ZnO nanocomposites [17]. Nevertheless, Sudakar et al. insisted that the observed RTFM in CuO/ZnO multilayers is largely contributed to CuO particle size, but not to the interfacial area between both oxides [18]. Therefore, more detailed researches are quite demanded to study the ferromagnetic property in CeO_2/CuO nanocomposite and further understand the ferromagnetic mechanism in such nonmagnetic composites, which will be of benefit to fill the above-mentioned existing research gaps and integrate ferromagnetic and photocatalytic property into the CeO_2/CuO nanocomposites for their development in multi-functions.

In this letter, CeO_2/CuO nanocomposites are fabricated with various

---

* Corresponding author.
E-mail address: pingwu@tju.edu.cn (P. Wu).

https://doi.org/10.1016/j.ceramint.2017.12.141
Received 4 December 2017; Received in revised form 18 December 2017; Accepted 19 December 2017

Please cite this article as: Ma, X., Ceramics International (2017), https://doi.org/10.1016/j.ceramint.2017.12.141

phase proportions by a one-step hydrothermal method. The work is mainly focused on investigating the structure, morphology, optical and magnetic property in CeO_2/CuO nanocomposite system. Ferromagnetism is observed firstly at the interface between CeO_2 and CuO, which manifests that introducing interfaces between two different oxide materials is effective to tailor the local electronic and magnetic order. The studies can give new insight into the understanding of RTFM origin and the design of multi-functional materials.

2. Experimental details

The analytical $CeCl_3·7H_2O$, $Cu(CH_3COO)_2·H_2O$ and urea were used as the starting materials to prepare the CeO_2/CuO nanocomposites via a hydrothermal reaction. Initially, $CeCl_3·7H_2O$ and $Cu(CH_3COO)_2·H_2O$ with different molar ratios (Ce:Cu = 2:1, 1:1, 1:2, 1:5) were dissolved in 20 mL deionized water to form transparent blue metal salt solution. Then 10 mL urea solution as the mineralizer was added, and the mixed solution instantly became vivid blue after urea solution addition. The mixture was continuously stirred for 30 min, then transferred into Teflon-lined stainless autoclave with 50 mL capacity and maintained in an oven at 140 °C for 4 h. After cooling, the obtained precipitate was washed by centrifugation with deionized water and absolute ethanol, subsequently dried at 60 °C for 12 h. For convenience, all as-synthesized CeO_2/CuO nanocomposites were named according to the phase proportions of CeO_2 and CuO as Ce2Cu1, Ce1Cu1, Ce1Cu2, Ce1Cu5. The fabrications of pure CeO_2 and pure CuO followed the same procedure for comparison purposes.

X-ray diffractometer (XRD, D/max-2500) was used to determine the phase structure and crystal lattice of the samples. The surface morphology and element distribution of the nanocomposites were observed through Field emission scanning electron microscopy (SEM, Nanosem 430) and Transmission electron microscopy (TEM, JEM-2100F). The valence states of ions and different bonded oxygen species in prepared products were characterized using X-ray photoelectron spectroscopy (XPS, PHI1600). The defects analyses were conducted by Raman spectrometer (Renishaw in Via-Reflex) equipped with 532 nm excitation source. The optical properties were measured using the UV–Vis–IR Lambda 750 Spectrophotometer and the magnetic properties were examined by the Quantum Design superconducting quantum interference device (SQUID, Quantum Design, MPMSXL-5).

3. Results and discussion

The XRD patterns of pure CeO_2 and CeO_2/CuO nanocomposites are presented in Fig. 1. The reflection peaks labeled as circle dots indicate face-centered cubic CeO_2 while diamonds correspond to monoclinic structured CuO. All of the diffraction peaks in as-prepared samples can be easily indexed to the CeO_2 and CuO phase, and no other peaks related to Ce_2O_3, Cu_2O, $(CeOH)CO_3$ or $Cu_2(OH)_2CO_3$ are detected within XRD detection limit, confirming CeO_2/CuO nanocomposites are successfully prepared. The variations of CeO_2 and CuO phase ratios can be reflected from the relative intensities of their diffraction peaks. However, for the sample Ce2Cu1, the intensities of CuO peaks are weaker, almost negligible, due to Cu ions incorporated into the CeO_2 lattice. With the proportion of CuO increasing gradually, the CuO diffraction peaks are readily observable, which is because Cu ions into CeO_2 reaches saturation and then extra Cu ions are transformed into CuO phase. Similar phenomena have been observed in recently reported CeO_2/CuO composites [8,20]. Avgouropoulos et al. concluded that the absence of CuO peaks in CeO_2/CuO (15 mol% CuO) sample is contributed to the amount of Cu^{2+} incorporated into the CeO_2 lattice forming solid solution [8]. For all samples, the average crystallite sizes of CeO_2 are determined to about 9–11 nm, according to Scherrer formula on the basis of the (111) diffraction peak of CeO_2.

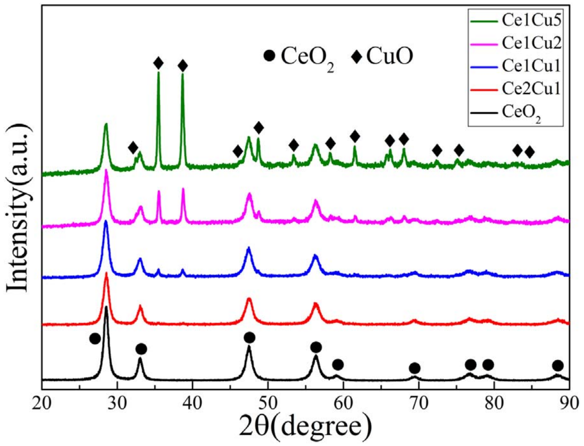

Fig. 1. XRD patterns for pure CeO_2 and CeO_2/CuO nanocomposites.

Fig. 2 illustrates the SEM micrographs of the pure CeO_2 and CeO_2/CuO nanocomposites. The pure CeO_2 presents irregular morphologies including self-assembled sheet-like and rod-like structure. It is obvious that Ce2Cu1 and Ce1Cu1 samples have almost similar morphology, only some extent of changes compared to pure CeO_2, showing Cu ions entering into CeO_2 lattice has little effect on the resulting morphology. But interestingly, the morphology of Ce1Cu2 almost completely turns into sheet-like structure, indicating the appearance of CuO phase severely affects the final morphology and increasing CuO content is more helpful for the formation of nanosheets. In order to get a deeper look at the microstructure, we have further achieved TEM images of Ce1Cu2. From Fig. 3(a), the TEM image of Ce1Cu2 consists of two morphologies: one is nanoparticle-like and the other is nanosheet-like structure, which can be clearly observed in the Fig. 3(b). To identify separately the location of CeO_2 and CuO in Ce1Cu2, sample is studied using the STEM technique. Fig. 3(c) displays the high-angle annular dark-field (HAADF)-STEM image taken from the square region of Fig. 3(a), and Fig. 3(d)–(f) show the elemental maps based on above STEM image. The mapping displays that nanosheets include only Cu elements and the distribution of Ce fits well with the nanoparticle segment, with oxygen being uniformly distributed over the whole sample. However, a little Cu is located at the nanoparticle segment as well owing to a certain amount of Cu ions doping into CeO_2 lattice, which is consistent with the XRD analyses. These above results clearly imply that Ce1Cu2 contains Ce, Cu and O elements, and the nanoparticle-like structure is self-aggregated CeO_2 crystallites and the nanosheet-like appearance is formed by the CuO. In the HRTEM analysis (Fig. 3(g)), the lattice fringes are clearly visible with interplanar spacings of ~ 0.31 nm and ~ 0.25 nm, which can be attributed to the (111) plane of CeO_2 and the (−111) plane of CuO, respectively. Furthermore, the contact interface zone between CuO and CeO_2 can be obviously observed.

The composition information and elementary oxidation state for representative sample of Ce1Cu2 are further investigated by XPS. All peaks in the survey scan spectrum (Fig. 4(a)) can be only assigned to Ce, Cu, O, and C elements, where the C 1*s* (284.6 eV) is applied to calibrate the binding energies in the XPS spectra during the test process. Therefore, the results verify again that there are no other impurities in the fabricated samples. Fig. 4(b) presents eight deconvoluted peaks in Ce 3*d* core level spectrum, where six Ce 3*d* binding energy peaks marked as U‴, U″, U, V‴, V″ and V correspond to $3d_{3/2}$ and $3d_{5/2}$ for Ce^{4+} states, whereas two weak peaks denoted as U′ and V′ refer to $3d_{3/2}$ and $3d_{5/2}$ for Ce^{3+} states [6,21,22]. This observation demonstrates that Ce^{4+} and Ce^{3+} coexist on the CeO_2/CuO samples, where the presence of Ce^{3+} is ascribed to charge transfer caused by the strong interaction of CeO_2 with CuO oxides. As a result of Ce^{4+} reduction, lots of oxygen vacancies are created and interface zone is the most preferred site of oxygen vacancies in oxide nanocomposites [23,24]. From Fig. 4(c), the two strong peaks for Cu 2*p* centered at about ~ 932.8 eV and ~ 952.6 eV with a spin-orbit splitting energy gap of 20 eV are assigned to